



Influence of Nucleation Layers on MOVPE Growth of Semipolar (11 $\bar{2}2$) GaN on *m*-Plane Sapphire

A. Azizur Rahman¹ · Nirupam Hatui¹ · Carina B. Maliakkal¹ · Priti Gupta¹ · Jayesh B. Parmar¹ · Bhagyashree A. Chalke¹ · Arnab Bhattacharya¹

Received: 18 November 2020 / Accepted: 20 April 2021 / Published online: 21 May 2021
© The Minerals, Metals & Materials Society 2021

Abstract

The influence of the underlying nucleation layer on the properties of semipolar (11 $\bar{2}2$) GaN grown on *m*-plane sapphire by metalorganic vapor-phase epitaxy has been investigated. (11 $\bar{2}2$) GaN epilayers of $\sim 1 \mu\text{m}$ thickness were grown using four different initiating sequences: low-temperature AlN and GaN, and high-temperature AlN buffer layers, and directly (high-temperature GaN). The choice of nucleation layer had a pronounced effect on the surface morphology and crystal quality of the overlying GaN epilayer. In comparison, direct growth of (11 $\bar{2}2$) GaN without any buffer layer provided the best crystal quality with a rocking-curve ω full-width at half-maximum (FWHM) value of 720 arcsec along the [11 $\bar{2}3$] direction and relatively enhanced near-band-edge photoluminescence emission, thus showing this direct growth process to be a simple route for synthesis of semipolar (11 $\bar{2}2$) GaN layers.

Keywords High-resolution x-ray diffraction · low-pressure metalorganic vapor-phase epitaxy · nitrides · semiconducting III–V materials

Introduction

Semipolar III-nitride layers are being extensively studied for reduced-polarization optoelectronic devices compared with conventional polar III-nitride layers grown on the *c*-plane orientation.^{1–3} While the best device results have been demonstrated on homoepitaxially grown layers on bulk semipolar GaN substrates,^{2,4,5} these substrates are usually of very small size and extremely expensive. Heteroepitaxial growth of semipolar GaN on easily available, large-area, and relatively cheap substrates is promising and has been the focus of many studies. Semipolar III-nitride layers can be grown on various foreign substrates, such as (1 $\bar{1}01$) GaN on 7° off-cut (001) silicon,⁶ (10 $\bar{1}\bar{1}$) GaN on (100) MgAl₂O₄,⁷ as {1 $\bar{1}01$ } side facets grown on *c*-plane GaN on sapphire,⁸ (10 $\bar{1}1$) GaN on graphene,⁹ (20 $\bar{2}1$) GaN on patterned (114) Si,¹⁰ (11 $\bar{2}0$) and (10 $\bar{1}3$) GaN on GaAs substrates,¹¹ (11 $\bar{2}2$)

and (10 $\bar{1}3$) GaN on *m*-plane sapphire,¹² or on facets of (0001) GaN stripes.¹³

Among the various substrate options, growth of GaN on *m*-plane sapphire has attracted much attention, since it does not require prior patterning and is readily commercially available. However, growth on *m*-plane sapphire can yield both (11 $\bar{2}2$) and (10 $\bar{1}3$) semipolar orientations, usually determined by the initial nitridation conditions.^{14–16} The (10 $\bar{1}3$) semipolar orientation suffers from the presence of a twinned (10 $\bar{1}3$) phase, thus the growth of (11 $\bar{2}2$) GaN has received more attention. The (11 $\bar{2}2$) orientation also offers both reduced polarization and high indium incorporation efficiency.¹⁷ However, semipolar (11 $\bar{2}2$) GaN films suffer from relatively poor crystalline quality and surface morphology because of the anisotropic in-plane lattice mismatch between semipolar (11 $\bar{2}2$) GaN and the (10 $\bar{1}0$) sapphire substrate.¹⁸ Thus, heteroepitaxially grown (11 $\bar{2}2$) GaN on *m*-plane sapphire typically has a high density of threading dislocation (TDs) of $\sim 10^{10} \text{ cm}^{-2}$ and basal plane stacking faults (BSFs) of $\sim 10^5 \text{ cm}^{-2}$.¹²

To optimize the growth of (11 $\bar{2}2$) GaN on *m*-plane sapphire via metalorganic vapor phase epitaxy (MOVPE), various approaches have been pursued. A two-temperature growth process was adopted^{14,19} with a low-temperature

✉ A. Azizur Rahman
azizur@tifr.res.in

¹ Department of Condensed Matter Physics and Material Science, Tata Institute of Fundamental Research, Mumbai 400 005, India

(LT) (610° to 620°C) nucleation layer followed by high-temperature (HT) GaN grown at 880° to 990°C . Wernicke et al.¹⁹ and Ploch et al.²⁰ showed that the substrate nitridation step was critical to obtain preferential $(11\bar{2}2)$ layers. In all these cases, the epilayers had a residual $(10\bar{1}3)$ phase amounting to almost $1/250$ of the $(11\bar{2}2)$ phase even for the best results. Sun et al.²¹ obtained better results using a HT-AlN nucleation layer in a multistep growth. In another approach, Kappers et al.²² used growth conditions similar to *c*-plane GaN, with a SiN_x interlayer in an attempt to improve the layer quality. Recently, Pristovsek et al.²³ showed much better phase purity when using SiN_x and multiple AlN interlayers. Improved layer quality has been obtained by the use of epitaxial lateral overgrowth techniques,^{24,25} especially asymmetrical lateral overgrowth,^{26–28} which promotes fast growth along *+c*-axis. Growth on prepatterned sapphire substrates,^{29,30} GaN nanorod templates,³¹ and use of In islands³² have also been attempted to improve layer quality, with mixed results. Recently, semipolar $(11\bar{2}2)$ GaN with better crystalline quality was obtained using *in situ* multiple ammonia treatment and insertion of *in situ* SiN_x interlayers.^{16,33} However, most approaches use either additional *ex situ* processing or complex *in situ* treatments.

A direct growth process has the advantage of being relatively simple. In $(11\bar{2}2)$ III-nitride growth, the nucleation layer plays a crucial role in determining the orientation as well as crystal quality and properties of the epilayer. In this work, $(11\bar{2}2)$ GaN epilayers were grown on different AlN and GaN nucleation layers and their influence on the microstructure, surface morphology, and optical properties of the epilayer studied.

Experimental Procedures

Semipolar $(11\bar{2}2)$ GaN layers were grown on different nucleation layers on epi-ready *m*-plane sapphire in a Thomas Swan $3 \times 2''$ closed-coupled showerhead MOVPE reactor. Trimethylgallium (TMGa), trimethylaluminum (TMAI), and ammonia (NH_3) were used as precursors, with Pd-diffused hydrogen (H_2) as carrier gas. The *m*-plane sapphire substrate was nitridated during the heat up while the temperature was ramped up to 1080°C in a mixture of NH_3 (1.5 slpm) and H_2 (8.5 slpm). The sapphire nitridation step is crucial for obtaining single-phase $(11\bar{2}2)$ GaN by suppressing the formation of mixed-phase $(10\bar{1}3)$.¹⁴ GaN epilayers were grown using four different nucleations: low-temperature AlN (sample A), high-temperature AlN (sample B), low-temperature GaN (sample C), and directly (high-temperature GaN, sample D). Growth conditions and thickness of the nucleation layers were chosen based on literature.^{3,21} All $(11\bar{2}2)$ GaN layers were grown at a temperature of 1080°C at reactor pressure of 6.7 kPa

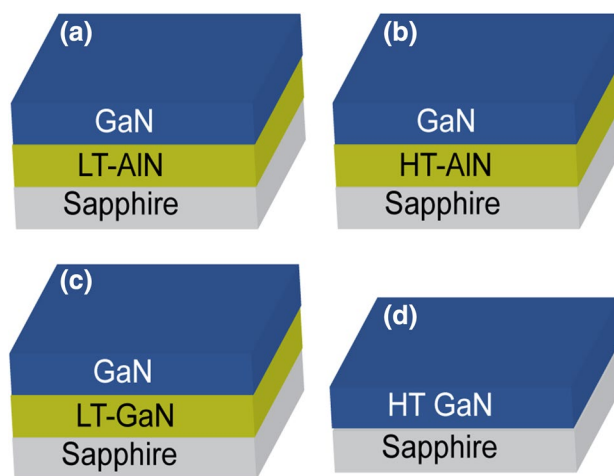


Fig. 1 Schematic representation of $(11\bar{2}2)$ GaN grown on (a) LT-AlN, (b) HT-AlN, (c) LT-GaN, and (d) no buffer.

Table 1 Parameters for different growth initiation sequences

| Sample | Buffer Layer | Temperature ($^{\circ}\text{C}$) | Pressure (kPa) | Thickness (nm) |
|--------|--------------|------------------------------------|----------------|----------------|
| A | LT-AlN | 600 | 6.7 | 60 |
| B | HT-AlN | 1080 | 6.7 | 500 |
| C | LT-GaN | 500 | 13.3 | 60 |
| D | No buffer | – | – | – |

(50 Torr) and V/III ratio of ~ 1200 . A schematic representation of $(11\bar{2}2)$ GaN grown using different nucleation layers is shown in Fig. 1. The growth parameters for the four samples are summarized in Table 1.

The growth was monitored *in situ* using a LayTec Epicurve TT normal-incidence reflectometer monitoring system, which uses a 635-nm light-emitting diode (LED) source. The microstructure of the sample, including the in-plane anisotropy, was examined using high-resolution x-ray diffraction (HRXRD) measurements performed on a PANalytical X'Pert diffractometer with an Eulerian cradle. The surface morphology of the layers was studied using atomic force microscopy (AFM) in noncontact mode and scanning electron microscopy (SEM), and the optical properties were measured using absorption and low-temperature (~ 10 K) photoluminescence (PL) spectroscopy. The luminescence was excited using a frequency-quadrupled Nd:YAG laser. The collected light was dispersed through a 0.55-m monochromator and detected with a cooled Si charge-coupled device (CCD) detector. Further, a transmission electron microscopy (TEM) investigation was also carried out at an accelerating voltage of 300 kV for our best sample to study the interface region between semipolar GaN and *m*-plane sapphire.

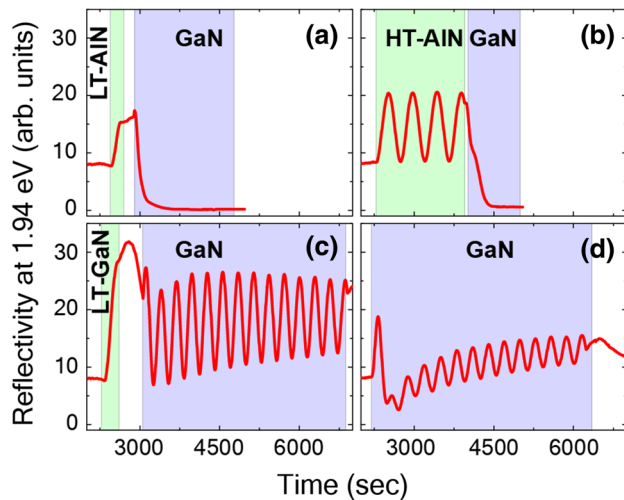


Fig. 2 *In situ* reflectance measurement at 1.94 eV of (11 $\bar{2}$) GaN grown on different buffer layers: (a) LT-AlN, (b) HT-AlN, (c) LT-GaN, and (d) no buffer.

In Situ Reflectance

Figure 2 shows the *in situ* optical reflectance traces (at $\lambda = 635$ nm) for the growth of GaN on different buffer layers. The reflectance trace for sample A shows a quick decay in reflectance once the TMGa is introduced into the reactor, indicating very high surface roughness. In sample B, growth of the HT-AlN layer shows undamped Fabry–Pérot oscillations (FPOs), but for GaN growth, the reflectance quickly drops to zero, indicating high surface roughness. The FPOs of sample C show well-defined oscillations during GaN growth, with the reflectance trace showing immediate recovery of FPOs after the growth of LT-GaN, indicating a quasi-two-dimensional (quasi-2D) growth mode. There is a small decrease in the overall amplitude, but the central value remains almost the same. Although sample D starts with an immediate oscillation, the reflectivity drops down and recovers back, showing a changeover from a three-dimensional (3D) to 2D growth mode. After recovery, it showed well-sustained oscillations, albeit with a smaller amplitude whose average value slowly increased.

Results and Discussion

X-Ray Diffraction

The samples were probed using symmetric HRXRD scans over a wide angular range to check for the presence of different crystal domains in the layer, in particular traces of the (10 $\bar{1}$ 3) phase, which are invariably also nucleated along with the desired (11 $\bar{2}$) phase.^{14,34} Figure 3 shows a part of these

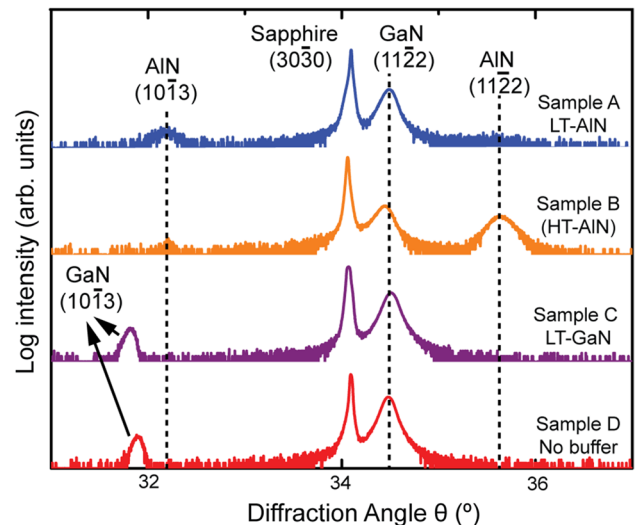


Fig. 3 Symmetric XRD $2\theta/\omega$ scans with the in-plane projection of the x-ray beam aligned parallel to (1100) GaN peak of the four GaN samples grown on different buffer layers.

$2\theta/\omega$ scans for the four GaN samples, with the *y*-axis plotted on a log scale to highlight low-intensity features. Besides the (11 $\bar{2}$) GaN and (30 $\bar{3}$ 0) sapphire peaks, we also see small peaks corresponding to (10 $\bar{1}$ 3)-oriented III-nitrides. For samples A and B grown on AlN buffer layers, the second GaN phase is not detectable, as also observed for growth on AlN layers,²³ although we see signatures of (10 $\bar{1}$ 3) AlN. Sample B also shows a prominent (11 $\bar{2}$) AlN peak from the buffer layer. For samples C and D, the presence of the (10 $\bar{1}$ 3) GaN phase is clearly visible, although the amount is estimated to be around 0.5%, roughly similar to values reported for (11 $\bar{2}$) GaN grown with GaN nucleation.²³

To evaluate the microstructure of (11 $\bar{2}$) GaN, it is necessary to measure x-ray rocking curves (XRCs) for multiple on- and off-axis reflections over sufficiently large azimuthal and inclination angles. Figure 4 shows the ω FWHM of the symmetric (11 $\bar{2}$) XRCs as a function of the azimuthal angle (ϕ) ($\phi = 0^\circ$ along $[\bar{1}100]$ *m*-axis, and 90° along $[\bar{1}\bar{1}23]$ projected-*c* direction). The anisotropic broadening of the on-axis (11 $\bar{2}$) XRCs is mainly due to the anisotropy in mosaic tilt and domain size.³⁵ Sample A grown on low-temperature AlN buffer shows an inverted trend of anisotropy, having higher FWHMs along the projected-*c* direction in contrast to the other samples. Samples C and D have low FWHM values along the projected *c*-axis, but sample C exhibits much higher anisotropy than sample D. As with any (11 $\bar{2}$) III-nitride grown on *m*-sapphire,³⁶ our epilayers are tilted about the $[1\bar{1}00]$ axis. This results in a difference in the FWHM values between $[\bar{1}\bar{1}23]$ and $[11\bar{2}\bar{3}]$ as the ω arc intercepts different lengths in reciprocal space. Thus, as inferred from these rocking curve measurements, sample D, having both less anisotropy and lower FWHM values (720 arcsec along

$[11\bar{2}\bar{3}]$ and 1340 arcsec along $[1\bar{1}00]$), has the best quality among these four samples. While the FWHM values are not smaller than those achieved for lateral overgrowth or using interlayers, they compare favorably with the best results obtained from two-step growth on *m*-plane sapphire^{19–21} (see Supplementary Information Table S1 for a comparison of x-ray rocking curve widths for growth using different approaches reported in literature).

Skew symmetric XRCs from the $(10\bar{1}1)$, $(10\bar{1}0)$, $(11\bar{2}0)$, and (0002) planes (inclination angle χ of approximately 26.0°, 42.5°, 31.6°, and 58.4° towards $(11\bar{2}2)$) were used to study the in-plane mosaicity of the epilayers²¹ and are plotted in Fig. 5. It shows a reduction in the FWHM of the XRCs by about 50% on moving from sample A to D, which again suggests that the direct high-temperature growth of GaN on sapphire provides the best microstructural quality of $(11\bar{2}2)$ GaN.

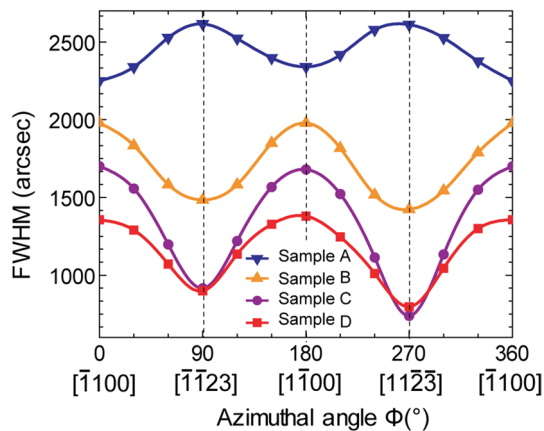


Fig. 4 XRD FWHM for on-axis XRC of $(11\bar{2}2)$ GaN as a function of azimuthal angle.

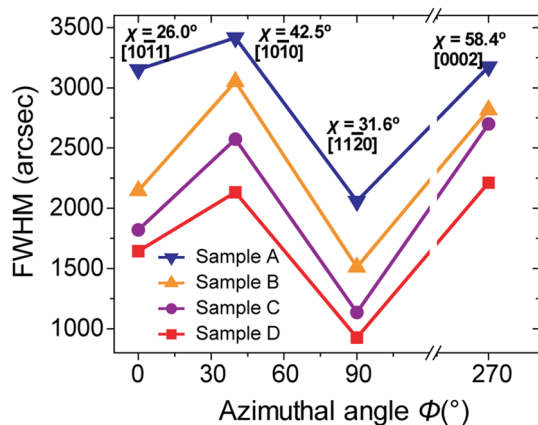


Fig. 5 XRD FWHM for off-axis XRC of $(11\bar{2}2)$ GaN as a function of azimuthal angle and inclination angle (lines are a guide to the eye).

Photoluminescence

Figure 6 shows the low-temperature PL spectra measured at ~ 10 K for all four samples. As commonly observed for semipolar alloys, the luminescence is dominated by emission from basal-plane stacking faults^{37–39} with the I_1 peak at 3.44 eV being the most prominent. Among all the samples, the direct growth (sample D) shows a relatively distinct near-band-edge feature at 3.49 eV due to emission from donor-bound excitons. The PL from prismatic stacking fault (PSF)-related emission is seen at 3.38 eV, and donor–acceptor pair (DAP) emission at 3.31 eV is also seen, with a small shoulder at 3.22 eV arising from the phonon replica. No significant yellow luminescence was observed from samples C and D (a longer wavelength range PL scan is shown in Supplementary Information Section 2, Figure S1).

A surprising observation is the high PL intensity at low temperature from sample A, which had an extremely rough surface and the largest XRD FWHM values. While we do not understand this, we speculate that this is simply an effect of better light outcoupling due to the rough surface or perhaps due to carrier confinement in localized regions formed by highly misaligned mosaic blocks.

Surface Morphology

The surface morphology of $(11\bar{2}2)$ GaN grown on different buffer layers was investigated using SEM and AFM. Representative SEM images of the samples are shown in Fig. 7. Sample A, grown on an LT-AlN buffer (Fig. 7a), exhibits a rough grainy surface structure, which correlates with the low optical reflectivity seen *in situ*. The

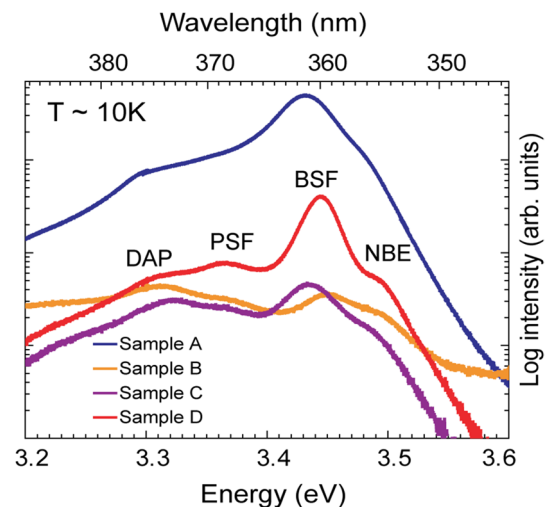


Fig. 6 Low-temperature PL spectra for samples A–D. Emissions from donor–acceptor pair (DAP), prismatic stacking fault (PSF), basal-plane stacking fault (BSF), and near-band-edge (NBE) are identified for sample D. The energies of the features are taken from Ref.¹⁹.

other buffer layers show the typical arrowhead features^{7,22} observed in semipolar GaN. The size of the arrowhead features is significantly smaller for both the LT-GaN and direct GaN growth in comparison with the HT-AIN growth. Sample C, grown on LT-GaN, shows long trenches along the projected *c*-direction. It has been speculated that the arrowhead features arise due to the tilt of the epilayers,¹⁹ although the absence of such arrowheads in other (11 $\bar{2}$ 2) III-nitrides where tilt is present³⁶ indicates that this

might not be the case. The arrowheads (for sample D) are typically about 2 μm in size, and the density is approximately $6 \times 10^7 \text{ cm}^{-2}$ to $7 \times 10^7 \text{ cm}^{-2}$ based on an analysis of SEM images.

A comparison of the AFM images of the morphology of the regions outside these trenches is shown in Fig. 8 (SEM comparison in Supplementary Information Section 3, Figure S2). Sample C is locally smoother, with a finer scale of the surface features and an root-mean-square

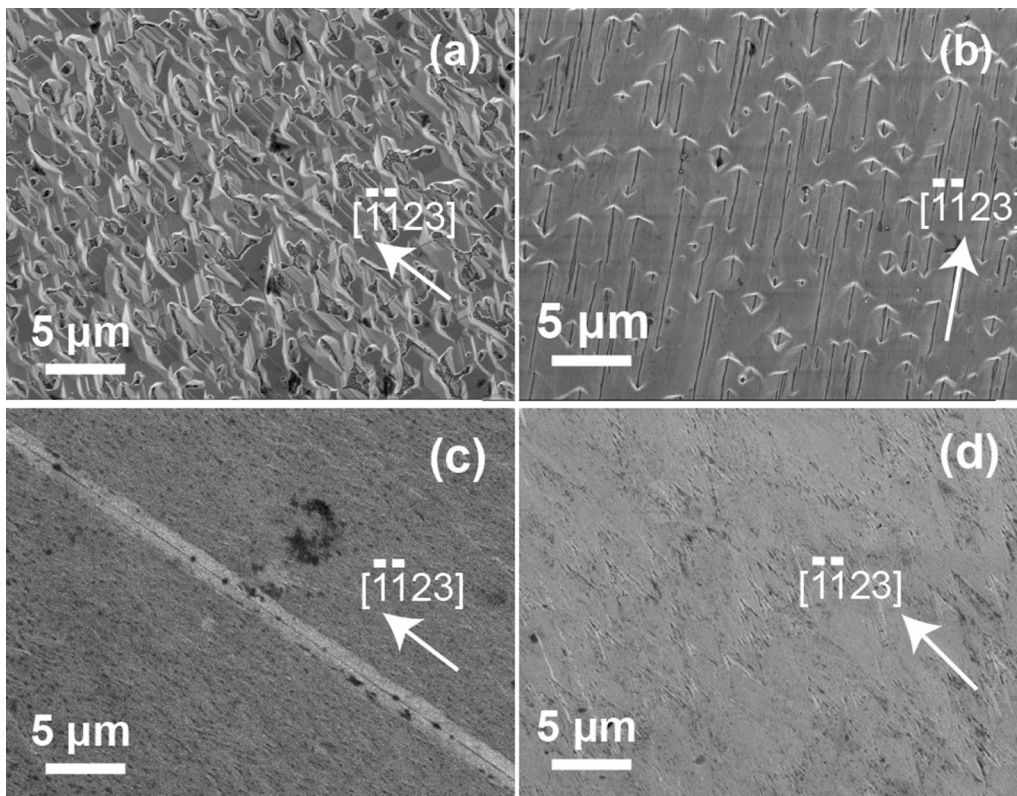


Fig. 7 SEM images of (11 $\bar{2}$ 2) GaN samples grown on different layers: (a) LT-AIN, (b) HT-AIN, (c) LT-GaN, and (d) no buffer.

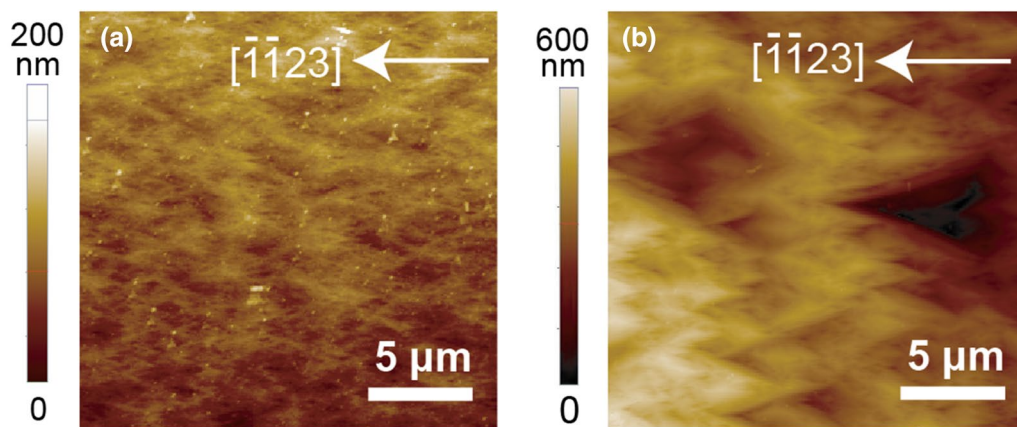


Fig. 8 AFM images of (11 $\bar{2}$ 2) GaN layers: (a) sample C (in the region outside the trenches) and (b) sample D.

(rms) roughness of ~ 20 nm, compared with sample D, which has well-defined arrowhead features and an RMS roughness of ~ 50 nm.

TEM of Interface Layer

High-resolution TEM investigations were performed on sample D. Cross-sectional TEM specimens were prepared by a conventional combination of mechanical grinding and ion milling, and the samples were imaged along the $[\bar{1}100]$ zone axis of GaN. Figure 9 shows a high-resolution image which reveals a strong contrast between the sapphire substrate, an interface region, and the GaN epilayer. Additional TEM images are shown in Supplementary Information Section 4 (Figs. S3 and S4). The density of BSFs was estimated to be $4 \times 10^{-6} \text{ cm}^{-1}$, close to values reported in literature^{23,28} (see Supplementary Information Fig. S3).

We also observed a continuous interface layer that formed as a result of the nitridation of the sapphire (the bright layer of ~ 3 nm thickness seen in Fig. 9). This is similar to earlier studies reporting an AlN layer at the sapphire–GaN interface in *c*-plane^{40,41} and semipolar $(1\bar{1}\bar{2}2)$ GaN.⁴² Nanobeam diffraction patterns obtained from the substrate, interface, and GaN epilayer also showed variations suggesting the presence of an interface layer with a change in composition (see Supplementary Information Fig. S5). Since the nitridation of sapphire is likely to introduce the diffusion of nitrogen atoms in Al_2O_3 , the composition near the interface would be some $\text{Al}_x\text{O}_y\text{N}_z$. Given that the layer is very thin, an exact compositional analysis is, however, difficult.

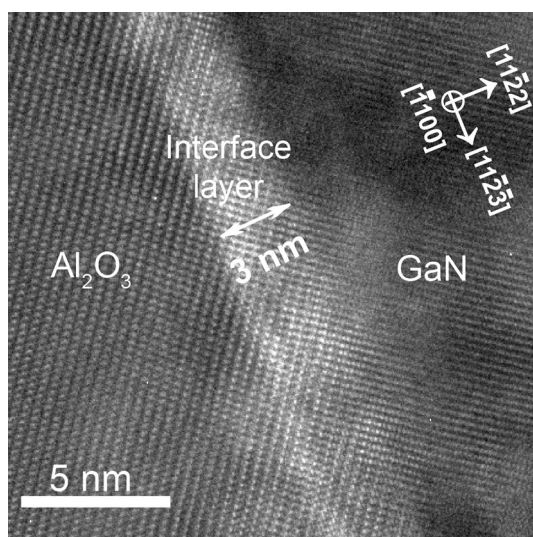


Fig. 9 HRTEM image of interface region between sapphire and GaN for sample D. The projection is along the $[\bar{1}100]$ GaN zone axis.

Conclusions

This comparative study of semipolar $(1\bar{1}\bar{2}2)$ GaN epilayers grown on different AlN and GaN buffer layers reveals that, under appropriate conditions, the direct growth of $(1\bar{1}\bar{2}2)$ GaN at high temperature on *m*-plane (i.e., without any buffer layer) provides the best crystal quality, albeit with a $\sim 0.5\%$ inclusion of $(10\bar{1}3)$ phase. We obtain layers with an FWHM value of 720 arcsec along the $(1\bar{1}\bar{2}3)$ direction for the on-axis rocking curve and relatively enhanced near-band-edge PL emission. This simple direct route for synthesis of $(1\bar{1}\bar{2}2)$ GaN layers would be useful for the development of semipolar materials and devices.

Supplementary Information The online version contains supplementary material available at <https://doi.org/10.1007/s11664-021-08969-7>.

Acknowledgments The authors are grateful to Sandip Ghosh for helpful discussions, Maheshwar Gokhale for help with HRXRD measurements, Amit P. Shah for help with PL measurements, and Rudheer D. Bapat and Shashank C. Purandare for help with TEM imaging of the sample. This work was supported by the Govt. of India through TIFR research grant 12P0168.

Conflict of interest The authors declare that they have no conflicts of interest.

References

1. F. Scholz, *Semicond. Sci. Technol.* 27, 024002 (2012).
2. R.M. Farrell, E.C. Young, F. Wu, S.P. DenBaars, and J.S. Speck, *Semicond. Sci. Technol.* 27, 024001 (2012).
3. T. Wang, *Semicond. Sci. Technol.* 31, 093003 (2016).
4. H. Zhong, A. Tyagi, N.N. Fellows, R.B. Chung, M. Saito, K. Fujito, J.S. Speck, S.P. DenBaars, and S. Nakamura, *Electron. Lett.* 43, 825 (2007).
5. H. Asamizu, M. Saito, K. Fujito, J.S. Speck, S.P. DenBaars, and S. Nakamura, *Appl. Phys. Express* 2, 021002 (2009).
6. T. Hikosaka, T. Narita, Y. Honda, M. Yamaguchi, and N. Sawaki, *Appl. Phys. Lett.* 84, 4717 (2004).
7. T.J. Baker, B.A. Haskell, F. Wu, P.T. Fini, J.S. Speck, and S. Nakamura, *Jpn. J. Appl. Phys.* 44, L920 (2005).
8. T. Wunderer, P. Bräckner, B. Neubert, F. Scholz, M. Feneberg, F. Lipski, M. Schirra, and K. Thonke, *Appl. Phys. Lett.* 89, 041121 (2006).
9. P. Gupta, A.A. Rahman, N. Hatui, M.R. Gokhale, M.M. Deshmukh, and A. Bhattacharya, *J. Cryst. Growth* 372, 105 (2013).
10. M. Khoury, M. Leroux, M. Nemoz, G. Feuillet, J. Zúñiga Pérez, and P. Vennéguès, *J. Cryst. Growth* 419, 88 (2015).
11. P. Saengkaew, S. Sanorpim, V. Yordsri, C. Thanachayanont, and K. Onabe, *J. Cryst. Growth* 411, 76 (2015).
12. T.J. Baker, B.A. Haskell, F. Wu, J.S. Speck, and S. Nakamura, *Jpn. J. Appl. Phys.* 45, L154 (2006).
13. K. Nishizuka, M. Funato, Y. Kawakami, S. Fujita, Y. Narukawa, and T. Mukai, *Appl. Phys. Lett.* 85, 3122 (2004).
14. S. Ploch, M. Frentrup, T. Wernicke, M. Pristovsek, M. Weyers, and M. Kneissl, *J. Cryst. Growth* 312, 2171 (2010).
15. K.R. Song, D.S. Oh, and S.N. Lee, *Curr. Appl. Phys.* 13, 1643 (2013).

16. A. Anuar, A.H. Makinudin, O. Al-Zuhairi, N. Chanlek, A.S. Bakar, and A. Supangat, *Vacuum* 174 (2020).
17. Y. Zhao, Q. Yan, C.Y. Huang, S.C. Huang, P.S. Hsu, S. Tanaka, C.C. Pan, Y. Kawaguchi, K. Fujito, C.G. Van de Walle, J.S. Speck, S.P. DenBaars, S. Nakamura, and D. Feezell, *Appl. Phys. Lett.* 100, 201108 (2012).
18. M. Frentrup, S. Ploch, M. Pristovsek, and M. Kneissl, *Phys. Status Solidi B* 248, 583 (2011).
19. T. Wernicke, C. Netzel, M. Weyers, and M. Kneissl, *Phys. Status Solidi C* 5, 1815 (2008).
20. S. Ploch, J.B. Park, J. Stellmach, T. Schwaner, M. Frentrup, T. Niermann, T. Wernicke, M. Pristovsek, M. Lehmann, and M. Kneissl, *J. Cryst. Growth* 331, 25 (2011).
21. Q. Sun, B. Leung, C.D. Yerino, Y. Zhang, and J. Han, *Appl. Phys. Lett.* 95, 1003 (2009).
22. M.J. Kappers, J.L. Hollander, C. McAleese, C.F. Johnston, R.F. Broom, J.S. Barnard, M.E. Vickers, and C.J. Humphreys, *J. Cryst. Growth* 300, 155 (2007).
23. M. Pristovsek, M. Frentrup, Y. Han, and C.J. Humphreys, *Phys. Status Solidi B* 253, 61 (2016).
24. X. Ni, Ü. Özgür, A.A. Baski, H. Morkoç, L. Zhou, D.J. Smith, and C.A. Tran, *Appl. Phys. Lett.* 90, 011002 (2007).
25. J.L. Hollander, M.J. Kappers, and C.J. Humphreys, *Physica B* 401, 307 (2007).
26. P. de Mierry, N. Kriouche, M. Nemoz, and G. Nataf, *Appl. Phys. Lett.* 94, 191903 (2009).
27. N. Kriouche, P. Vennéguès, M. Nemoz, G. Nataf, and P. de Mierry, *J. Cryst. Growth* 312, 2625 (2010).
28. S. Jang, H. Kim, D.S. Kim, S.M. Hwang, J. Kim, and K.H. Baik, *Appl. Phys. Lett.* 103, 162103 (2013).
29. B. Leung, Q. Sun, C. Yerino, Y. Zhanga, J. Hana, B.H. Kongb, H.K. Chob, K.Y. Liaoc, and Y.L. Lic, *J. Cryst. Growth* 341, 27 (2012).
30. M. Caliebe, T. Meisch, B. Neuschl, S. Bauer, J. Helbing, D. Beck, K. Thonke, M. Klein, D. Heinz, and F. Scholz, *Phys. Status Solidi C* 11, 525 (2014).
31. K. Xing, Y. Gong, X. Yu, J. Bai, and T. Wang, *Jpn. J. Appl. Phys.* 52, 08JC03 (2013).
32. C. Jung, J. Jang, J. Hwang, J. Jeong, J. Kim, K. Lee, and O. Nam, *J. Cryst. Growth* 370, 26 (2013).
33. K. Xing, C. Tseng, L. Wang, P. Chi, J. Wang, P. Chen, and H. Liang, *Appl. Phys. Lett.* 114, 131105 (2019).
34. N. Hatui, M. Frentrup, A.A. Rahman, A. Kadir, S. Subramanian, M. Kneissl, and A. Bhattacharya, *J. Cryst. Growth* 411, 106 (2015).
35. M.A. Moram, C.F. Johnston, J.L. Hollander, M.J. Kappers, and C.J. Humphreys, *J. Appl. Phys.* 105, 113501 (2009).
36. N. Hatui, A.A. Rahman, C.B. Maliakkal, and A. Bhattacharya, *J. Cryst. Growth* 437, 1 (2016).
37. R. Liu, A. Bell, F.A. Ponce, C.Q. Chen, J.W. Yang, and M.A. Khan, *Appl. Phys. Lett.* 86, 021908 (2005).
38. C. Netzel, J. Stellmach, M. Feneberg, M. Frentrup, M. Winkler, F. Mehnke, T. Wernicke, R. Goldhahn, M. Kneissl, and M. Weyers, *Appl. Phys. Lett.* 104, 051906 (2014).
39. J. Lähnemann, U. Jahn, O. Brandt, T. Flissikowski, P. Dogan, and H.T. Grahn, *J. Phys. D Appl. Phys.* 47, 423001 (2014).
40. P. Vennéguès, Z. Bougrioua, and T. Guehne, *Jpn. J. Appl. Phys.* 46, 4089 (2007).
41. P. Vennéguès and B. Beaumont, *Appl. Phys. Lett.* 75(26), 4115 (1999).
42. M. Biedermann, J.B. Park, T. Niermann, S. Ploch, M. Kneissl, and M. Lehmann, (HR)TEM study of the interface region between semi-polar GaN and *m*-plane sapphire. *Proceedings of the 15th European Microscopy Congress, 16th-21st September 2012, Manchester, UK. PSI.2* (2012). http://www.emc2012.org.uk//documents/Abstracts/Abstracts/EMC2012_0125.pdf.

Publisher's Note Springer Nature remains neutral with regard to jurisdictional claims in published maps and institutional affiliations.